Coupling Agent Effect on Magnetic Properties of Functionalized Magnetite-Based Nanoparticles

T. J. Daou,[†] J. M. Grenèche,[‡] G. Pourroy,[†] S. Buathong,[†] A. Derory,[†] C. Ulhaq-Bouillet,[†] B. Donnio,[†] D. Guillon,[†] and S. Begin-Colin*,[†]

Institut de Physique et Chimie des Matériaux, UMR 7504 CNRS-ULP, 23 rue du Loess, BP 43, 67034 Strasbourg Cedex 2, France, and Laboratoire de Physique de L'Etat Condensé, UMR CNRS 6087, Université du Maine, 72085, Le Mans Cedex 9, France

Received May 23, 2008. Revised Manuscript Received July 1, 2008

The effect of surface inorganic−organic interactions on magnetic and structural properties of iron oxide magnetic nanoparticles functionalized by lipophilic stilbene molecules has been investigated. The molecules have been grafted through either phosphonate or carboxylate coupling agents. Mössbauer spectra recorded at 300 and 77K suggest a global composition of $Fe_{2.82}O_4$ for the two types of functionalization. Complementary in-field Mössbauer and SQUID measurements have demonstrated that the nanoparticles consist in a magnetite core surrounded by an oxidized layer. The oxidized shell exhibits a spin canting in the carboxylate case leading to a decrease of the net magnetization of the oxide nanoparticle. No canting occurs in the phosphonate case, and the magnetic properties are therefore preserved. The magnetic properties thus depend on the coupling agent, e.g., surface interactions. This result is of primary importance to tune the magnetic properties of functionalized nanoparticles for biomedical and high density storage media applications.

1. Introduction

Functionalization of magnetic iron oxide nanoparticles by organic molecules gives rise to intensive research for biomedical applications such as magnetic drug targeting, cancer treatment (hyperthermia), enzyme immobilization, or magnetic resonance imaging,[1,2] as well as for a bottom-up approach to build nanodevices such as high density storage systems.[3] Indeed, for in vivo application as well as for nanoparticle self-assembly, the functionalization step is of fundamental importance to ensure suspension stability and to bring bioactive or structuring functions. For these technological applications, the grafting of the molecules at the surface of nanoparticles should occur while preserving the properties of both molecules and nanoparticles. However, most studies deal with the influence of the nanoscale on magnetic properties and few of them have been devoted to the specific effect of the organic coating and especially to the surface modification it generates.[4−7]

In most studies conducted mainly on maghemite nanoparticles, a decrease in the value of the saturation magnetization has been observed and then attributed to finite size effect, structural disorder in the whole particle and to surface effects, these latter being assigned to a large fraction of surface subcoordinated atoms and/or a disordered (spin-glass) or magnetically different surface layer, inducing spin canting. [8−21]

* Corresponding author. Fax: (33) 3.88.10.72.47. Tel.: (33) 3.88.10.71.92. E-mail: begin@ipcms.u-strasbg.fr.

[†] Institut de Physique et Chimie des Matériaux, UMR 7504 CNRS-ULP.

[‡] Laboratoire de Physique de L'Etat Condensé, UMR CNRS 6087.

(1) (a) Pankhurst, Q. A.; Connolly, J.; Jones, S. K.; Dobson, J. J. *Phys. D: Appl. Phys.* **2003**, *36*, R167. (b) Gupta, A. K.; Gupta, M. *Biomaterials* **2005**, *26*, 3995. (c) Mornet, S.; Vasseur, S.; Grasset, F.; Duguet, E. *J. Mater. Chem.* **2004**, *14*, 2161. (d) Arruebo, M.; Fernanfez-Pacheto, R.; Ibarra, M. R.; Santamaria, J. *Nanotoday* **2007**, *2*, 22. (e) Lu, A.-H.; Salabas, E. L.; Schüth, F. *Angew. Chem., Int. Ed.* **2007**, *46*, 1222.

(2) Tartaj, P.; Morales, M. P.; Veintemillas-Verdaguer, S.; Gonzales-Carreno, T.; Serna, J. C. *J. Phys. D: Appl. Phys.* **2003**, *36*, R182.

(3) (a) Reiss, G.; Hütten, A. *Nat. Mater.* **2005**, *4*, 725. (b) Guo, Q.; Teng, X.; Rahman, S.; Yang, H. *J. Am. Chem. Soc.* **2003**, *125*, 630. (c) Chen, H. Y. *Electrochem. Com.* **2006**, *8*, 148. (d) Fried, T.; Shemer, G.; Markovich, G. *Adv. Mater.* **2001**, *13*, 1158. (e) Poddar, P.; Fried, T.; Markovich, G. *Phys. Rev. B* **2002**, *65*, 172405. (f) Zeng, H.; Black, C. T.; Sandstrom, R. L.; Rice, P. M.; Murray, C. B.; Sun, S. *Phys. Rev. B* **2006**, *73*, 020402.

(4) Vestal, C. R.; Zhang, Z. J. *J. Am. Chem. Soc.* **2003**, *125*, 9828.

(5) Brice-Profeta, S.; Arrio, M. A.; Tronc, E.; Menguy, N.; Letard, I.; Cartier dit Moulin, C.; Nogues, M.; Chaneac, C.; Jolivet, J. P.; Sainctavit, Ph. *J. Magn. Magn. Mater.* **2005**, *288*, 254.

(6) Tronc, E.; Ezzir, A.; Cherkaoui, R.; Chanéac, C.; Noguès, M.; Kachkachi, H.; Fiorani, D.; Testa, A. M.; Grenèche, J. M.; Jolivet, J.P. J. *Magn. Magn. Mater.* **2000**, *221*, 63.

(7) Yee, C.; Kataby, G.; Ulman, A.; Prozorov, T.; White, H.; King, A.; Rafailovich, M.; Sokolov, J.; Gedanken, A. *Langmuir* **1999**, *15*, 7111.

(8) Morales, M. P.; Veintemillas, S.; Montero, M. I.; Serna, C. J.; Roig, A.; Casas, L. I.; Martinez, B.; Sandiumenge, F. *Chem. Mater.* **1999**, *11*, 3058.

(9) Dormann, J. L.; Tronc, E.; Fiorani, D. *Magnetic Relaxation in Fine-Particle Systems*; Advances in Chemical Physics Series; John Wiley and Sons: New York, 1997; Vol. 98.

(10) Tronc, E.; Prené, P.; Jolivet, J. P.; Dormannn, J. L.; Grenèche, J. M. *Hyperfine Interact.* **1998**, *112*, 97.

(11) Morrish, A. H.; Haneda, K. J. *Appl. Phys.* **1981**, *52*, 2496.

(12) Marco, M. D.; Port, M.; Couvreur, P.; Dubernet, C.; Ballirano, P.; Sadun, C. J. *Am. Chem. Soc.* **2006**, *128*, 10054.

(13) Morales, M. P.; Andres-Verges, M.; Veintemillas-Verdaguer, S.; Montero, M. I.; Serna, C. J. *J. Magn. Magn. Mater.* **1999**, *203*, 146.

(14) Coey, J. M. D. *Phys. Rev. Lett.* **1971**, *27*, 1140.

(15) Kodama, R. H.; Berkowitz, A. E. *Phys. Rev. B.* **1999**, *59*, 6321.

(16) Kodama, R. H.; Berkowitz, A. W.; McNiff, E. J.; Foner, S. *Phys. Rev. Lett.* **1996**, *77*, 394.

(17) Iglesias, O.; Labarta, A. *Phys. Rev. B* **2001**, *63*, 184416.

(18) Morales, M. P.; Serna, C. J.; Bodker, F.; Morup, S. *J. Phys.: Condens. Matter* **1997**, *9*, 5461.

(19) Parker, F. T.; Foster, M. W.; Margulies, D. T.; Berkowitz, A. E. *Phys. Rev.* **1993**, *47*, 7885.

10.1021/cm801405n CCC: $40.75
Published on Web 08/22/2008

It is well-established that the magnetic properties of nanoparticles are strongly dependent on their size but various synthesis routes may provide nanoparticles of similar grain size with different magnetic properties. In fact, the discrimination between finite size and surface effect contributions is not easy. In addition, one may notice that the specific influence of the organic bonding on magnetic properties has been not much investigated. Understanding the effect of the surface chemistry modification induced by ligand coordination on the structural and magnetic properties of functionalized magnetic iron oxide nanoparticles is also necessary for developing efficient magnetic functionalized nanoparticles. The spin canting noticed in $NiFe_2O_4$ nanoparticles covered by oleic acid has been first attributed to surface interactions with oleic acid through carboxylic groups and then to a core−shell structure, the core made of aligned spin and the shell of a spin-glass-like surface layer.[16] Such a magnetically disordered surface layer has also been observed in phosphated maghemite nanoparticles due to the formation of an iron phosphate surface complex, whereas no surface complex has been identified in sulfated maghemite nanoparticles.[5,6] Ngo et al.[22] observed a decrease in saturation magnetization of 3 nm cobalt ferrite nanoparticles after citrate coating, whereas an increase is reported with 4, 12, and 25 nm cobalt ferrites nanoparticles covered with substituted benzenes ($Y-C_6H_5$ with $Y = COOH$, SH, NH_2, OH, SO_3H) and substituted benzoic acid ligands ($HOOC-C_6H_4-R$ with $R = H$, CH_3, Cl, NO_2, OH),[4] and no change in polyphosphate treated γ-Fe_2O_3.[23] The reasons for such discrepancies are not entirely clear and influence of particle size, particle morphology, and nanoparticle composition are generally advanced.

Technological applications of magnetic nanoparticles require the understanding of the influence of surface chemistry modifications on the magnetic properties. The present study aims at emphasizing the effect of the coupling agent, i.e., the inorganic−organic interactions, on the magnetic properties of ferrimagnetic functionalized magnetite nanoparticles. Because of their grain size (39 ± 5 nm), these nanoparticles are well-suited to consider the volume effect mainly as the surface to volume ratio becomes small and as the temperature of Verwey transition, characteristic of nonsuperparamagnetic magnetite and sensitive to the particle size and deviation from stoichiometry, may be used to control the structural properties.[24] The influence of inorganic−organic interactions is thus investigated by deeply and carefully characterizing the magnetite nanoparticles grafted with stilbene molecules using either a carboxylate or a phosphonate group as coupling agent. The carboxylate group is usually used to connect molecules on oxide surfaces. The phosphonate one has been first involved in self-assembled monolayers (SAM) formation on metallic and metal oxide surfaces as protective films or for biomedical applications[25] and recently in the grafting of bioactive molecules.[7,26] The phosphonate group has been recently shown to allow a higher grafting density of stilbene molecules at the surface of the nanoparticles than the carboxylate group.[27] Here the effect of these two coupling agents, e.g., the surface chemistry, on the magnetite nanoparticle structure and the magnetic properties is investigated by ^{57}Fe in-field Mössbauer spectrometry, SQUID measurements, and IR spectroscopy.

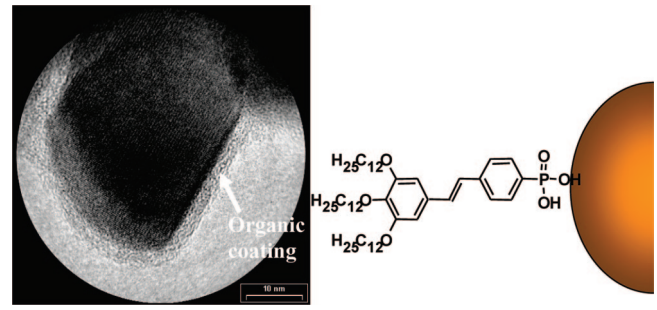

Figure 1. HRTEM micrograph of functionalized magnetite-based nanoparticles and stylized structure of phosphonated stilbene molecules.

2. Experimental Section

Synthesis of Magnetite Nanoparticles. Magnetite-based nanoparticles with an average grain size of 39 ± 5 nm (specific surface: 31 m^2/g) have been prepared in two steps by coprecipitation at 70 °C of Fe^{2+} and Fe^{3+} ions by a tetramethylammonium hydroxide ($(CH_3)_4OH$) solution, followed by an hydrothermal treatment at 250 °C as reported.[24] Their mean composition, $Fe_{2,95}O_4$, and their structure, a core of stoichiometric magnetite with an outer layer of substoichiometric magnetite, have been determined by X-ray diffraction, zero-field-cooled/field-cooled (ZFC/FC) magnetic measurements and ^{57}Fe Mössbauer spectrometry.[24]

Functionalization Step. One-hundred milligrams of nanoparticles were dispersed into 100 mL of tetrahydrofuran (THF) and 25 mg of stilbene molecules (the structure of phosphonated molecule is reported in Figure 1) was added. The grafting reaction was carried out at room temperature with mechanical stirring for 24 h. The grafted nanoparticles were magnetically decanted and washed three times with THF. The grafting and washing steps were identical for both molecules.

The amounts of grafted organic molecules have been evaluated indirectly by UV spectroscopy on washing solutions and directly by chemical analyses (CNRS analysis center of Vernaison) on dried grafted nanoparticles.

The corresponding carboxylated and phosphonated magnetite nanoparticles will be named in the text below C and P nanoparticles, respectively.

(20) Martinez, B.; Obradors, X.; Balcells, Bl.; Rouanet, A.; Monty, C. *Phys. Rev. Lett.* **1998**, *80*, 181.
(21) Roca, A. G.; Morales, M. P.; Grady, K.; Serna, C. J. *Nanotechnology* **2006**, *17*, 2783.
(22) Ngo, A. T.; Bonville, P.; Pileni, M. P. *Eur. Phys. J. B* **1999**, *9*, 583.
(23) Spada, F. E.; Parker, F. T.; Nakakura, C. Y.; Berkowitz, A. E. *J. Magn. Magn. Mater.* **1993**, *120*, 129.
(24) Daou, T. J.; Pourroy, G.; Bégin, S.; Grenèche, J. M.; Ulhacq, C.; Leuvrey, C.; Legaré, P.; Bernhardt, P.; Rogez, G. *Chem. Mater.* **2006**, *18*, 4399.
(25) (a) Guerero, G.; Mutin, P. H.; Vioux, A. *Chem. Mater.* **2001**, *13*, 4367. (b) Mutin, P. H.; Lafond, V.; Popa, A. F.; Granier, M.; Markey, L.; Dereux, A. *Chem. Mater.* **2004**, *16*, 5670. (c) Mutin, P. H.; Guerrero, G.; Vioux, A. *J. Mater. Chem.* **2005**, *15*, 3761. (d) Textor, M.; Ruiz, L;.; Hofer, R.; Rossi, A.; Feldman, K.; Haehner, G.; Spencer, N. D. *Langmuir* **2000**, *16*, 3257.
(26) (a) Frantz, R.; Granier, M.; Durand, J. O.; Lanneau, G. F. *Tetrahedron Let.* **2002**, *43*, 9115. (b) Kar, S.; Durand, J. O.; Granier, M.; Joly, P.; Melnyk, O. *Tetrahedron Let.* **2003**, *44*, 5617. (c) Sahoo, Y.; Pizem, H.; Fried, T.; Golodnitsky, D.; Burstein, L.; Sukenik, C. N.; Markovich, G. *Langmuir* **2001**, *17*, 7907. (d) De Silva, S. S.; Camp, P. J.; Henderson, D. K.; Henry, D. C. R.; McNab, H.; Tasker, P. A.; Wight, P. *Chem. Commun.* **2003**, *14*, 1702.
(27) Daou, T. J.; Buathong, S.; Ung, D.; Donnio, B.; Pourroy, G.; Guillon, D.; Bégin, S. *Sens. Actuators, B* **2007**, *126*, 159.

Table 1. Amount of Grafted Molecules Deduced Indirectly from UV Spectroscopy and Directly from Chemical Analyses[a]

	chemical analysis		UV analysis	
sample	carbon (wt %)	phosphorus (wt %)	carbon (wt %)	phosphorus (wt %)
starting nanoparticles	0.37 ± 0.01	0.00		
C nanoparticles	2.60 ± 0.08		2.60 ± 0.08	
P nanoparticles	4.20 ± 0.12	0.23 ± 0.07	4.17 ± 0.12	0.22 ± 0.01

[a] The amount of carbon due to the grafted organic molecules has been calculated by subtracting the total carbon amount by the amount of carbon in the starting nanoparticles and has been compared to the expected amount of carbon from indirect UV analysis.

Materials Characterization. The particles before and after grafting were characterized by X-ray diffraction (XRD) using a Siemens D-500 X-ray diffractometer with high intensity Co Kα radiation (25 mA, 35 kV) ($\lambda = 1.789$ Å), by transmission electron microscopy TEM with a TOPCON model 002B transmission electron microscope, operating at 200 kV, with a point-to-point resolution of 0.18 nm.

^{57}Fe Mössbauer spectra were recorded at 300 K and at 77 K using a conventional constant acceleration transmission spectrometer with a ^{57}Co(Rh) source and a bath cryostat. In-field spectra were recorded by means of a cryomagnetic device where the 8 T external magnetic field is applied parallel to the γ-radiation on the sample, the source remaining unpolarized. The spectra were fitted by means of the MOSFIT program (Teillet, J.; Varret, F. unpublished MOSFIT program, Université du Maine) and an α-Fe foil was used as calibration sample. The values of isomer shift (IS) are quoted to that of α-Fe at 300K.

ZFC/FC measurements were performed using a superconducting quantum interference device (SQUID) magnetometer (Quantum Design MPMS-XL model) between 4 and 400 K under a field of 10 Oe. The calibration was performed with a Pt sample provided by Quantum Design. Hysteresis cycles were recorded at room temperature by using a vibrating sample magnetometer.

3. Results and Discussions

3.1. Structural Characterization. The amount of organic molecules, which have not been grafted, has been evaluated by UV spectroscopy from washing solutions and a calibrating curve and then the grafting rate has been deduced. The amount of grafted organic molecules was found to be 1.4 and 0.85 molecule/nm^2 for the phosphonated and the carboxylated molecules, respectively. These amounts of grafted organic molecules have also been confirmed by chemical analyses performed on grafted nanoparticles (Table 1). The specific area surface of nanoparticles and the surface of both molecules being 31 m^2/g and 0.72 nm^2, respectively, it leads to a surface covering of about 100% with phosphonated molecules and about 61% with the carboxylated one.

Magnetite is an inverse spinel: $Fe^{3+}{}_A[Fe^{2+}Fe^{3+}]_BO_4{}^{2-}$. The Fe^{2+} ions in octahedral (O_h) sites are very sensitive to oxidation. The oxidation of Fe^{2+} into Fe^{3+} is accompanied by vacancy formation (□), giving the general formula $Fe^{3+}{}_A[Fe^{2.5+}{}_{2-6\delta}Fe^{3+}{}_{5\delta}\square_\delta]_BO_4{}^{2-}$. The complete oxidation corresponds to $\delta = 1/3$ and leads to maghemite. The XRD patterns of magnetite and maghemite are very similar and the lattice parameter must be precisely determined. The XRD patterns of the magnetite nanoparticles grafted with stilbene molecules using a phosphonate and carboxylate group as coupling agent are characteristic of a spinel ferrite. The lattice parameter of magnetite before grafting is equal to $a = 0.8393(5)$ nm and close to the stoichiometric magnetite one (0.8396 nm, JCPDS file 19−629). It decreases down to $a = 0.8388(5)$ nm and $a = 0.8380(5)$ nm for phosphonated and carboxylated nanoparticles, respectively. These values are closer to that of stoichiometric magnetite than that of maghemite (0.8346 nm, JCPDS file 39−1346), suggesting thus that few Fe^{2+} cations have been oxidized.[24,28]

From Mössbauer spectra at 300 K (figure 2) and 77 K (not shown here), a mean composition of $Fe_{2.82}O_4$ has been determined for both carboxylated and phosphonated nanoparticles. This confirms that an oxidation of Fe^{2+} has occurred during the grafting step, in agreement with X-ray diffraction. However, as already observed on magnetite nanoparticles and detailed in an earlier study on phosphated magnetite nanoparticles, this deviation from stoichiometry may originate from the surface of nanoparticles, the core remaining stoichiometric.[24,28] The discrepancy between the spectra at 77 K and those recorded on γ-Fe_2O_3−Fe_3O_4 solid solutions with similar stoichiometry deviation by Schimdbauer and Keller[29] allows us to conclude that the grafted nanoparticles are not such solid solutions. The temperature dependencies of the ZFC and FC magnetization also give information on the stoechiometry of magnetite because the Verwey transition temperature (T_V) is very sensitive to deviation from stoechiometry.[30] The ZFC curves of grafted magnetite nanoparticles, given in Figure 3, display the two transition temperatures usually observed in bulk monocrystalline stoichiometric magnetite: one located at around 120 K corresponding to the Verwey transition temperature of stoichiometric magnetite,[31] and the other at about 50 K, attributed to a relaxation process.[32] The value of the Verwey transition temperature (T_V) at 120 K is thus found to correspond to that reported for bulk magnetite. This value of T_V and Mössbauer results confirm that only the surface of functionalized nanoparticules does present a deviation from stoichiometry and that the main volume is constituted of stoichiometric magnetite. These results lead us to describe nanoparticles as a core of stoichiometric magnetite surrounded by an oxidized layer (Figure 4). Such a description is in agreement with the model developed by P. Perriat and al.[33] for oxidation in finely divided ferrites: upon oxidation, the bulk is subjected to increasingly compressive stresses so that, in the bulk, the diffusion is strongly decreased and even comes to a stop. This results in a core−shell structure with an oxidized shell (Fe_2O_3) and a nonoxidized core (Fe_3O_4).

(28) Daou, T. J.; Bégin-Colin, S.; Grenèche, J. M.; Thomas, F.; Derory, A.; Bernhardt, P.; Legaré, P.; Pourroy, G. *Chem. Mater.* **2007**, *19*, 4494.
(29) Schmidbauer, E.; Keller, M. J. *Magn. Magn. Mater.* **2006**, *297*, 107.
(30) Guigue-Millot, N.; Keller, N.; Perriat, P. *Phys. Rev. B* **2001**, *64*, 012402.
(31) Aragon, R.; Shepherd, J. P.; Koenitzer, J. W.; Buttrey, D. J.; Rasmussen, R. J.; Honig, J.M. J. *Appl. Phys.* **1985**, *57*, 3221.
(32) Skumryev, V.; Blythe, H. J.; Cullen, J.; Coey, J. M. D. *J. Magn. Magn. Mater.* **1999**, *19*, 6197–515.
(33) (a) Perriat, P.; Domenichini, B.; Gillot, B. J. *Phys. Chem. Solids* **1996**, *57*, 1641. (b) Guigue-Millot, N.; Champion, Y.; Hÿtch, M. J.; Bernard, F.; Bégin-Colin, S.; Perriat, P. J. *Phys. Chem. B* **2001**, *105*, 7125.

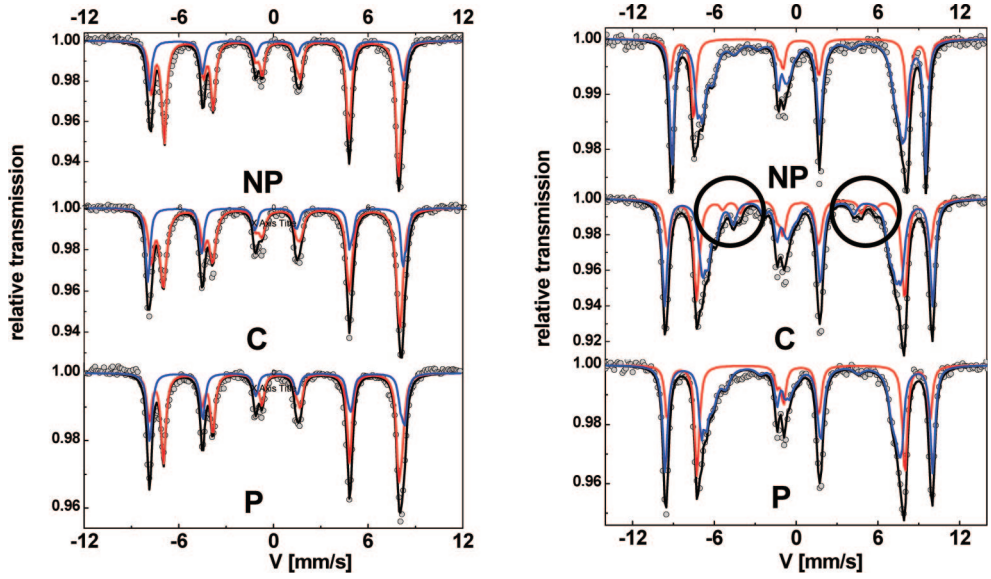

Figure 2. Mössbauer spectra of as-prepared (NP) and C and P nanoparticles recorded at 300 (left) and 10 K (right) in the presence of an 8 T external magnetic field applied parallel to the radiation. The fitting model assumes the presence of both stoichiometric magnetite and maghemite.

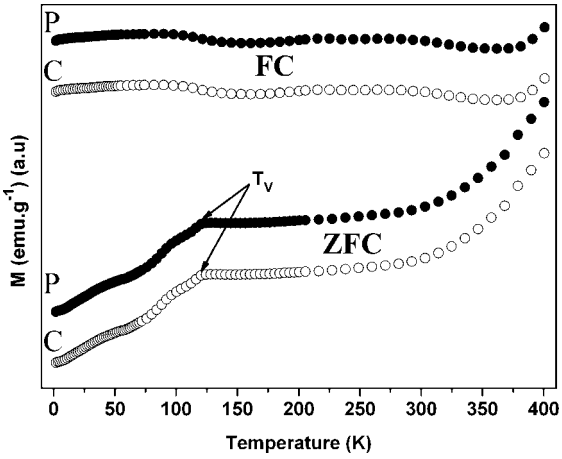

Figure 3. ZFC/FC curves of P and C nanoparticles under a field of 10 Oe.

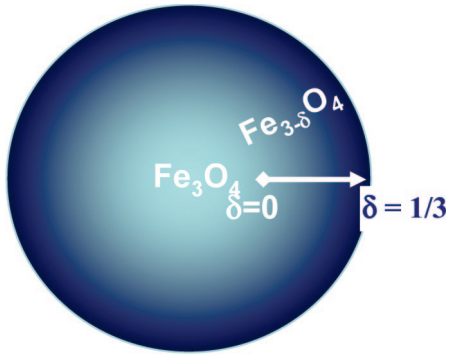

Figure 4. Structural description/scheme of functionalized magnetite nanoparticles.

To evaluate the thickness of the oxidized layer, a second fitting procedure of Mössbauer spectra recorded at 300 K involving both stoichiometric magnetite and maghemite, was successfully achieved (Table 2). It is then found, considering the same value of recoil-free factor that the best fit of hyperfine structure corresponds to a fraction of about 64 ± 3% and 66 ± 3% of magnetite and 36 ± 3% and 34 ± 3% of maghemite for C- and P nanoparticles, respectively. Assuming a core−shell (magnetite-maghemite) description and a diameter equal to 39 nm, the thickness of the maghemite shell would be about 2.8(3) and 2.6(3) nm for the C and P nanoparticles, respectively, corresponding thus to about 4 elementary cells. Such an approach can also be a priori applied at 77 K, but remains less accurate and less reasonable from a fitting point of view, because of the rather complex hyperfine structure of magnetite below the Verwey transition. It is thus concluded that this modeling approach can be successfully applied only on Mössbauer spectra recorded above the Verwey transition: in this temperature range, the characteristic time of electronic hopping between Fe^{2+} and Fe^{3+}, $\sim 1 \times 10^{-9}$ s, is slightly smaller than the available time for the Mössbauer spectrometry, giving rise to a well defined sextet for Fe located in octahedral sites.[14] It is important to emphasize that this ideal two-phase description suggests rather that the core of nanoparticles does consist of a stoichiometric magnetite and is surrounded by an oxidized layer with an increase of the oxygen content from the inner to the outer part (Figure 4).

The same analyses performed on the initial magnetite nanoparticles give 75% of magnetite and a maghemite surface layer 1.8 nm thick. The oxidized layer certainly displays an oxidation gradient from the surface to the core. Nevertheless, such a modeling approach allows to evaluate an order of magnitude of the layer thickness and leads to a fairly realistic fit of the Mössbauer spectra instead of considering a magnetite phase only. Indeed, the later approach would lead to unexpected tetrahedral to octahedral Fe ratios and to a decrease of the isomer shift of the tetrahedral Fe sites.[24]

A higher oxidation rate is observed in the functionalized nanoparticles by comparison with starting and phosphated magnetite nanoparticles.[28] The composition of phosphated nanoparticles was found to remain close to that of the starting magnetite because of the strong affinity of phosphorus-based ions toward metals or metal (hydr)oxides. Indeed, the

Table 2. Refined Values of Hyperfine Parameters Estimated from ^{57}Fe Mössbauer Spectra at 300 K on Nonfunctionalized (NP) and C and P Nanoparticles[a]

		IS (mm s^{-1}) ± 0.01			2ε (mm s^{-1}) ± 0.01			B_{hf} (T) ± 0.3			relative absorption (area %) ± 1.0		
		NP	C	P	NP	C	P	NP	C	P	NP	C	P
300 K	γ-Fe_2O_3T O	0.29	0.29	0.29	0*	0*	0*	49.4	49.7	49.0	9.2	13.5	13.0
		0.40	0.39	0.39	0*	0*	0*	50.0	50.3	50.0	15.5	22.5	21.6
	Fe_3O_4 T O	0.31	0.31	0.31	0.01	0*	0*	48.7	49.1	49.5	25.1	21.3	21.8
		0.66	0.65	0.66	0.01	−0.01	−0.01	45.7	46.2	46.1	50.2	42.6	43.6

[a] The fitting model assumes the presence of both stoichiometric magnetite and maghemite. IS, 2ε, B_{hf}, and % correspond to the isomer shift, quadrupole shift, hyperfine field, and relative absorption area, respectively.

phosphatation occurs rapidly and the phosphate coating acts further as a corrosion/oxidation inhibitor.[28] The larger oxidized surface layer encountered with the present C and P nanoparticles may be explained by a less dense surface coverage with stilbene molecules and thus a less efficient protective layer. Indeed, the maximum amount of grafted molecules is lower in stilbene grafted nanoparticles (1.4 molecule/nm^2 (surface coverage of ∼ 100%) and 0.85 molecule/nm^2 (surface coverage of ∼ 61%) for the phosphonated and the carboxylated molecules, respectively) than in phosphated nanoparticles (3.3 phosphate molecules/nm^2) because of a larger area of the stilbene molecules (0.72 nm^2) with respect to the phosphate ones (0.24 nm^2). Moreover, the higher grafting rate with the phosphonate coupling agent with respect to the carboxylate one was assigned to a stronger bonding at the surface of nanoparticles.

3.2. Characterization of the Oxidized Surface Layer. The amorphous organic coating has been observed at the surface of nanoparticles by TEM (Figure 1). The thickness of this layer corresponds to the length of the organic molecules, 3 nm, confirming a monolayer covering of magnetite nanoparticles.

Another way to characterize the oxidized layer can be achieved by IR spectroscopy, as both magnetite and maghemite can be easily differentiated on symmetry grounds. Wavenumbers assigned to spinel structure are in the 800−400 cm^{-1} range. The IR spectra of stoichiometric magnetite display one peak at around 570 cm^{-1}, whereas the IR spectra of maghemite are more complicated due to the sensitivity of IR analyses to vacancies ordering (Figure 5). Indeed, maghemite ($Fe^{3+}{}_A[Fe^{3+}{}_{5/3}\square_{1/3}]_BO_4{}^{2-}$) differs from magnetite by the presence of vacancies within the Oh sites, and the absence of Fe^{2+} cations. It often displays superstructure forms, which arise as a result of cationic and vacancy ordering. The vacancies can be randomly distributed (space group *Fdm* as in magnetite), or partially ($P4_332$) or totally ordered ($P4_32_12$).[2,34−36] Infrared spectroscopy has been shown to be very sensitive to the order−disorder and the higher the order, the larger the number of lattice absorption bands between 800 and 200 cm^{-1} (Figure 5).[2,8,13,36] Maghemite with vacancy disordering exhibits IR spectrum with two broad features at around 600 and 450 cm^{-1}, assigned respectively to Fe−O deformation in O_h and T_d sites and Fe−O deformation in O_h sites.[13] The vacancy ordering

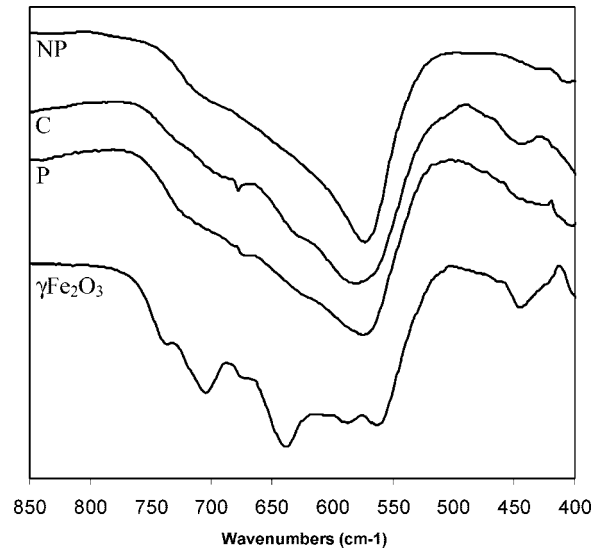

Figure 5. IR spectra of as-prepared (NP) and C and P nanoparticles and of maghemite in the Fe−O wavenumber range. The maghemite phase has been obtained by heating the magnetite nanoparticles under air at 300 °C.

is reported to change the symmetry of the spinel phase or to appear without distortion of the cubic cell, consequently revealing additional absorption bands between 700 and 500 cm^{-1} (Figure 5). IR spectra of magnetite and phosphonated and carboxylated magnetite in the 900−400 cm^{-1} range are given in Figure 5. The IR spectrum of magnetite displays an intense band at around 570 cm^{-1} with a large shoulder up to 750 cm^{-1}. Considering the aforementioned earlier IR spectroscopy studies and the microstructure of magnetite nanoparticles with a magnetite core and an oxidized layer, the intense band at 570 cm^{-1} is attributed to magnetite and the very broad shoulder to that of the oxidized layer with a composition close to that of a disordered maghemite.

Further Mössbauer analyses on functionalized magnetite nanoparticles have been undertaken under an external magnetic field of 8T applied parallel to the γ-beam. The intensity of the second and fifth lines of the magnetic sextet gives clear evidence for Fe moment direction with respect to the applied field: the average canting angles derive from the ratios of the line intensities of $A_{2,5}$ to $A_{1,6}$ (external lines) according to the following relation: $\beta = \arcsin[(3A_{2,5}/2)A_{1,6}/(1 + 3A_{2,5}/4A_{1,6})]^{1/2}$.[37] The in-field Mössbauer spectra of both functionalized nanoparticles are compared to those of the non functionalized ones in Figure 2. Both profiles and intensities of outer and inner lines are rather similar, but one can observe changes in the intermediate lines: naked and phosphonated nanoparticles behave as a collinear ferrimagnet,

(34) Morales, M. P.; Pecharroman, C.; Gonzales-Carreno, T. J. *Solid State Chem.* **1994**, *108*, 158.
(35) Greaves, C. J. *Solid State Chem.* **1983**, *49*, 325.
(36) Belin, T.; Guigue-Millot, N.; Caillot, T.; Aymes, D.; Niepce, J.C. J. *Solid State Chem.* **2002**, *163*, 459.
(37) Greneche, J. M. *Acta Phys. Slov.* **1995**, *45*, 45.

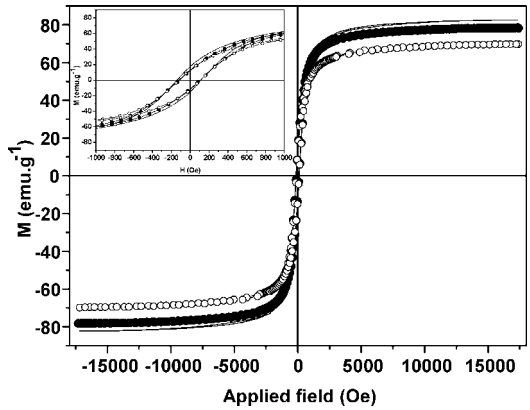

Figure 6. Magnetization curves at 300 K of as-prepared (black line) and C (○) and P (•) nanoparticles.

whereas a canted ferrimagnetic structure occurs in the case of magnetite nanoparticles grafted with carboxylated molecules. Considering different fitting models involving canted magnetic structures of magnetite and/or maghemite phases, we conclude unambiguously that only the maghemite component attributed to the external shell is canted. The angle values are found to be about 25(8)° for both tetrahedral and octahedral Fe magnetic moments, corresponding to an average uniform canted layer of about 0.55(15) nm. It is important to emphasize that this magnetic thickness of about two atomic layers well corroborates previous results observed at the surface of nanoparticles[6,10,11] and at the interface grain−amorphous remainder in nanocrystalline alloys.[38]

3.3. Magnetic Measurements. As spin canting generally modifies the magnetic properties, the magnetic behavior of grafted nanoparticles has been studied and compared to that of as-prepared nanoparticles. Magnetization curves are plotted as a function of an applied field in Figure 6. Once the organic weight contribution has been subtracted, the saturation magnetization of as-prepared and C and P magnetite nanoparticles is found to be 83, 72, and 83 emu/g, respectively. Let us note that the saturation magnetization of the magnetite nanoparticles is lowered after functionalization with the carboxylate molecules unlike the phosphonate ones, for which it is not affected. Similar results were previously observed after phosphatation of 39 nm magnetite nanoparticles, whatever the phosphatation rate. To get a better insight on the surface structure, the saturation magnetization of the oxidized layer has been calculated.

The whole saturation magnetization can be expressed as the sum of the contributions of the stoichiometric core and maghemite layer following the equation:

$$Ms = Ms_{Fe_3O_4}(=92\ \text{emu/g})(\%\ \text{of magnetite}) + Ms_{\text{oxidized layer}}(\%\ \text{of maghemite}) \quad (1)$$

Taking into account the ratio of each phase given in Table 2, the saturation magnetization of the oxidized layer has been calculated and is equal to 36.8, 54.4, and 65.0 emu g^{-1} for the carboxylated, as-prepared, and phosphonated magnetite nanoparticles, respectively. These values are significantly lower than that of bulk maghemite (74 emu/g) and may not be explained by only an oxidation gradient within the oxidized layer instead of a maghemite layer. Indeed, a strong decrease of the saturation magnetization of the oxidized layer is thus noticed for C nanoparticles in agreement with the spin canting observed by in-field Mössbauer spectrometry. For the phosphonated nanoparticles, no spin canting has been observed and the saturation magnetization in the layer is slightly higher by comparison with that of the as-prepared nanoparticles in spite of a larger oxidized layer. Both phosphonated and carboxylated magnetite-based nanoparticles display an oxidized layer and a narrow mean composition, whereas the canting is observed only with the carboxylated one. It is thus concluded that the phosphonate coupling agent enhances the magnetic properties (increase of the magnetic order) in the oxidized layer and that the nature of the coupling agent and its interaction with the surface layer is at the origin of the observed canting. In addition, the thickness of the canted layer in C nanoparticles is about 0.55(15) nm, whereas the oxidized layer thickness is about 2.8(3) nm. Thus the decrease in the saturation magnetization is certainly due to the contribution of the oxidized layer and a canted surface layer in this oxidized layer.

In the case of as-prepared nanoparticles, the decrease in Ms of the oxidized layer (by comparison with Ms of maghemite) may be explained by a magnetically dead surface layer (unnoticeable by Mössbauer spectroscopy). According to these observations, a schematic representation of the surface of nanoparticles explaining the different observed magnetic properties is proposed in Figure 7. The surface spin disorder is often suggested to arise from reduced coordination of surface cations and broken exchange bonds between surface spins, giving rise to magnetic frustration.[5,14,16,17,19]

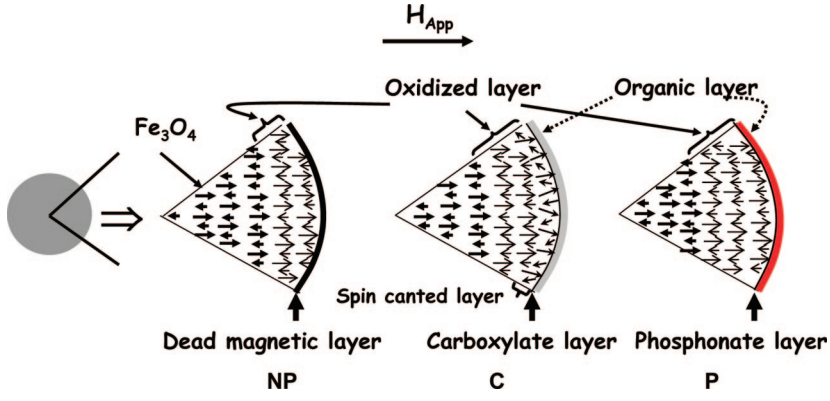

Figure 7. Schematic representation of the surface of as-prepared (NP) and C and P nanoparticles in the presence of an applied magnetic field. Arrows depict the resultant ferrimagnetic moment.

Numerical calculations show that broken exchange bonds are sufficient to induce surface spin disorder.[16,17] Indeed, a surface layer should break partially the ferrimagnetic correlation. Spin canting induced by broken exchange bonds would imply that carboxylate interactions limit the surface exchange bonds, whereas the phosphonate ones allow further superexchange magnetic interactions. This hypothesis is supported by the fact that carboxylate molecules are often reported to be coordinated to the oxide surfaces via a chelate complex [4,39,40] while monodentate or bridging bidentate complexes are often identified with phosphonate molecules depending on the pH.[6,7,41] The surface of nanoparticle displaying subcoordinated cations, phosphonate groups at the surface of nanoparticles should take the positions of the missing oxygen atoms, making the symmetry and the crystal field of the surface closely resembling that of the core and therefore reducing the spin disorder. To ascertain this proposal, we have to further identify the surface complexes. The morphology as well as the chemical and electronic states of the surface of the as-prepared nanoparticles, are crucial parameters to understand and model the physical and chemical bonding after grafting molecules. Further experimental studies are now in progress.

4. Conclusion

Magnetite-based nanoparticles 39 nm in size have been used to get a better understanding of the effect of the surface chemistry modification induced by ligand coordination. The magnetic structure of the oxide surface layer on which functional molecules have been grafted depends on the nature of the coupling agent through which the molecules are linked to the surface. The carboxylate coupling agent induces a spin canting in the oxidized layer reducing the saturation magnetization. On the contrary, there is no canted surface structure when phosphonated molecules are linked covalently onto the iron oxide nanoparticles. This is of particular importance to keep the magnetic properties unchanged when nanoparticles have to be coated with an organic layer.

CM801405N

(38) Slawska-Waniewska, A.; Greneche, J. M. *Phys. Rev. B* **1997**, *56*, R 8491.
(39) Zhang, L.; He, R.; Gu, H. C. *Appl. Surf. Sci.* **2006**, *253*, 2611.
(40) Marinescu, G.; Patron, L.; Culita, D. C.; Neagoe, C.; Lepadatu, C. I.; Balint, I.; Bessais, L.; Cizmas, C.B. J. *Nanopart. Res.* **2006**, *8*, 1045.
(41) (a) Barja, B. C.; Tjedor-Tjedor, M. I.; Anderson, M. A. *Langmuir* **1999**, *15*, 2316. (b) Persson, P.; Nilsson, N.; Sjöberg, S. *J. Colloid Interface Sci.* **1996**, *177*, 263. (c) Elzinga, E. J.; Sparks, D.L. J. *Colloid Interface Sci.* **2007**, *308*, 53.